Rotorcraft-pilot coupling analysis through state-space aerodynamic modelling

J. Serafini
serafini@uniroma3.it
Roma Tre University
Department of Engineering
Rome
Italy

L. Greco
CNR-INSEAN
Marine Technology Research Institute
Rome
Italy

M. Gennaretti
Department of Engineering
Roma Tre University
Rome
Italy

ABSTRACT

The terminology 'rotorcraft-pilot coupling' denotes phenomena arising from interaction between pilot and rotorcraft. Among these, the present work deals with 'pilot-assisted oscillations' that derive from unintentional pilot actions on controls due to seat vibrations, and are strictly related to rotor-aeroelasticity/airframe-structural-dynamics coupling, with involvement of blade control actuator dynamics. Focusing the attention on helicopters, a comprehensive rotorcraft model is developed and applied, with main rotor unsteady aerodynamics described in state-space form. This makes it particularly suited for stability and frequency-response analysis, as well as control applications. Numerical investigations address two critical rotorcraft-pilot coupling aeroelastic issues: stability of vertical bouncing and gust response in hovering. Results from main rotor unsteady aerodynamics modelling are compared with widely-used quasi-steady aerodynamics predictions. These suggest that, for accurate RPC/PAO phenomena predictions, mathematical modelling should include the three-dimensional, unsteady-flow effects, and that the pilot-in-the-loop passive behaviour produces a beneficial effect on the load factor generated by gust encountering.

Paper No. 4274. Manuscript received 9 October 2014, revised version received 15 February 2015, second revised version received 21 April 2015, accepted 21 April 2015.

https://doi.org/10.1017/S0001924000011155 Published online by Cambridge University Press

NOMENCLATURE

$\mathbf{A}_0,\mathbf{A}_1,\mathbf{A}_2,\mathbf{A},\mathbf{B},\mathbf{C}$	rational-approximation matrices
a_0, a_z	vertical acceleration of pilot hand and pilot seat
D, ω_θ	equivalent relative damping and frequency of actuator dynamics
$\mathbf{E}_b$, $\mathbf{E}$	blade and rotor aerodynamic matrices
$\mathbf{f}_{aer}$	blades generalised aerodynamic forces
$\mathbf{f}_{hub}$	main rotor hub loads
$\mathbf{f}_{str}^{ex,nl}$	nonlinear structural and inertial forces due to non-blade dofs
$\mathbf{f}_\xi$	generalised forces on airframe modes
G	gain parameter of pilot transfer functions
g	gravity acceleration
H	transfer function between seat acceleration and stick motion
$\mathrm{I}_{ij}^k = I_{ij}/I_{kk}$	nondimensional components of airframe inertia matrix
N_a	number of additional aerodynamic states
N_b	number of main rotor blades
N_f	number of generalised aerodynamic forces
N_m	number of generalised coordinates of blade elastic motion
$\mathbf{M},\mathbf{C},\mathbf{K}$	rotor mass, damping and stiffness structural matrices
M_f	helicopter mass
$\mathbf{M}_\xi,\mathbf{C}_\xi,\mathbf{K}_\xi$	airframe mass, damping and stiffness matrices
$\mathbf{q}$	blade elastic motion generalised coordinates (N_m)
$\mathbf{r}$	main rotor aerodynamic states (N_a)
r_{st},α	collective stick length and rotation
u,v,w,p,q,r	entries of column matrix $\boldsymbol{\zeta}$
$\vec{v}_{rig}$	blade rigid-body velocity
$\vec{v}_{def}$	blade deformation velocity
$\vec{v}_\theta$	blade velocity due to pitch control
$\vec{v}_H$	hub velocity
$\mathbf{v}$	rotor rigid-body motion generalised velocities
X,Y,Z,L,M,N	airframe forces and moments about centre of gravity
$\boldsymbol{\zeta}$	airframe rigid-body linear and angular velocities
$\boldsymbol{\theta}_c$	blade pitch controls
θ_0	blade collective pitch control
$\boldsymbol{\xi}$	airframe deformation dofs
ϕ,θ,ψ	roll, pitch and yaw angles
$\vec{\Phi}_l$	shape functions of blade deformation
$\vec{\Psi}_n$	shape functions of rotor rigid-body motion velocity
$\vec{\omega}$	rotor angular velocity

1.0 INTRODUCTION

Rotorcraft-Pilot Couplings (RPCs) are a wide class of phenomena arising from unwanted interaction between pilot and rotorcraft. These undesirable couplings may produce instabilities which negatively affect ride qualities, structural strength requirements and sometimes can generate catastrophic accidents. RPCs are usually divided into two main categories: Pilot-Induced Oscillations (PIO) occurring when the pilot, attempting to perform a given task,

https://doi.org/10.1017/S0001924000011155 Published online by Cambridge University Press

inadvertently excites divergent vehicle oscillations by applying control inputs that are in the wrong direction or have phase lag with aircraft motion, and Pilot-Assisted Oscillations (PAO) that are the result of involuntary pilot control inputs due to his body motion response to vibrations and accelerations[1-3].

Following an earlier interest in the field of fixed-wing aircraft, recently RPC phenomena have captured increasing attention by the rotorcraft research community, designers and operators. In particular, the European research project ARISTOTEL (2010-2013) aimed at defining appropriate tools for the prediction of proneness of modern aircraft and rotorcraft to adverse pilot coupling, and identifying guidelines for designers of next generation aircraft to avoid it[2-4]. RPC analysis is a very complex task that involves rigid body dynamics, aeroservoelasticity, flight control systems and, of course, piloting and biodynamic feedthrough (BDFT – involuntary motion of body parts, such as limbs and hands, due to vehicle vibrations and accelerations, that may lead to involuntary control inputs)[2]. In PAO problems, an important role is played by main rotor aeroelasticity[2,5].

Most of the research effort focused on helicopter modelling for RPC analysis has been based on sectional, quasi-steady models for the simulation of main rotor airloads[6,7], although more recently three-dimensional, fully unsteady aerodynamic models have been applied in RPC time-marching responses[8-10]. Work related to RPC experimental investigation and simulation modelling is also presented in Refs 11 and 12. In addition, a linearised aeroelastic main rotor model suitable for helicopter stability analysis in the presence of RPC has been introduced in Ref. 13. It yields hub loads transmitted to the airframe as functions of hub motion and pilot controls, with blades degrees of freedom implicitly represented by internal dynamics poles[13].

Focusing the attention on helicopters, the objective of this work is the development of a linear state-space numerical tool for the analysis of RPC phenomena, particularly suitable for stability analysis and control applications. The capability of response analysis is limited to small perturbations, thus excluding prediction of limit-cycle phenomena. It is based on the finite-state main rotor unsteady aerodynamics modelling presented in Ref. 14, and further applied in Ref. 15 for proprotor whirl flutter analysis. This state-space unsteady aerodynamic model is obtained through a frequency-domain aerodynamic solver yielding sampling of the transfer functions between blade airloads and degrees of freedom, followed by their rational-matrix approximation. This approach is closely related to the well known Karpel method[16] for fixed-wing aerodynamics, and inspired by the pioneering work in Refs 17-19.

The influence of different aerodynamic models in predicting pilot-in-the-loop aeroelastic stability and gust responses is examined. Simulations using unsteady aerodynamics are compared with those derived through quasi-steady aerodynamics with wake-inflow downwash corrections. The attention is focused on PAO phenomena with dynamics characteristic frequencies in the range 2-8Hz, where the rotorcraft response is dominated by the interplay between rotor blades aeroelasticity and airframe dynamics. In particular, the numerical investigation concerns the problem known as 'vertical bouncing', which is a PAO instability caused by the coupling, through the pilot, of vertical acceleration with collective control stick movement[7,20]. The response of a piloted helicopter in hovering condition to vertical and lateral gusts (of interest in many applications and missions, such as rescue, patrolling and positioning of loads) is also examined.

2.0 RPC PHENOMENOLOGY

RPCs include a wide class of phenomena that involve the interplay of structural dynamics, rigid body dynamics, aeroservoelasticity, automatic flight control system and, of course, piloting and BDFT.

https://doi.org/10.1017/S0001924000011155 Published online by Cambridge University Press

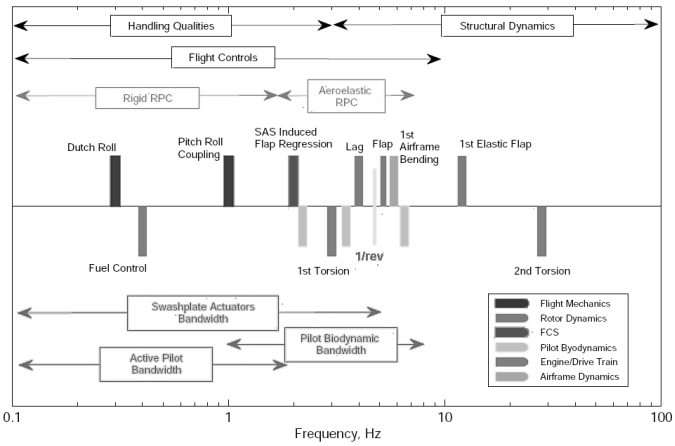


Figure 1. Typical frequencies of rotorcraft dynamics[10].

The outcomes of the research activity developed under the European project ARISTOTEL confirmed the definition of two main classes of RPCs (rigid-body RPC and aeroelastic RPC), on the basis of the prevalent dynamics involved and the corresponding frequency ranges of interest (approximately 0-2Hz and 2-8Hz, respectively)[2-4]. As mentioned above, these are also strictly related to the type of feedback exerted by the pilot: in the 0-2Hz frequency range RPC is dominated by voluntary (active) intervention that inadvertently excites vehicle oscillations giving rise to the so-called PIO phenomena, whereas in the 2-8Hz frequency range the pilot provides (passive) involuntary control inputs due to seat vibrations and accelerations, giving rise to PAO events. Figure 1, taken from Ref. 10, shows a sketch of frequency ranges characterising the dynamics of the subsystems of a typical medium-weight helicopter. It is worth noting that typical pilot BDFT bandwidth overlaps with the frequency range where aeroelastic phenomena, and hence unsteady aerodynamic effects, are relevant. The width of the frequency range of transition from rigid-body to aeroelastic RPCs depends on BDFT and aeromechanical responses, with an important role played by the low-frequency flap modes.

In consideration of the extremely wide range of different RPC events that may occur, akin to the classification adopted for vehicle-pilot phenomena concerning fixed-wing aircraft, it has been proposed to group RPC phenomena into the following categories[2]:

- Category I: linear dynamic behaviour of piloted rotorcraft;
- Category II: quasi-linear dynamic behaviour of piloted rotorcraft, with nonlinearities induced by, for example, rate and/or position limiting control elements;
- Category III: essentially nonlinear dynamic behaviour of piloted rotorcraft, with PIOs triggered by switching during flight from one state to a different one (for instance, AFCS mode switching, task switching or changes in the aerodynamic configurations or in the propulsion system).

In addition, ARISTOTEL presented a selection of the most common aeroelastic RPC events that includes flexible airframe mode couplings, vertical bouncing via collective feedback, vertical bouncing via cyclic feedback, engine-drive train couplings and slung load-helicopter couplings[2].

https://doi.org/10.1017/S0001924000011155 Published online by Cambridge University Press

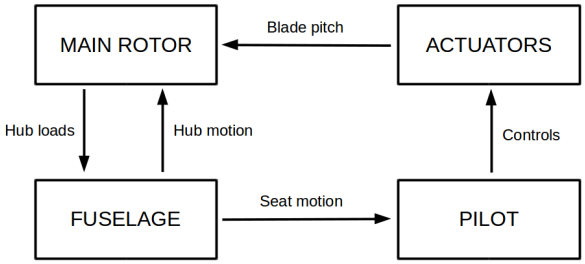


Figure 2. Block diagram of the interactions between model elements.

3.0 COMPREHENSIVE HELICOPTER MODELLING FOR PAO ANALYSIS

Detailed modelling of a helicopter is a difficult task that requires simulation of many complex structural and aerodynamic interactions among components, taking into account the necessary level of modelling accuracy and, at the same time, limiting the number of system variables involved. For the purposes of the present work, the comprehensive tool that has been developed considers the interplay among the components that significantly affect RPC onset. Figure 2 shows a block diagram that illustrates these components and their interactions.

In particular, main rotor aeroelasticity interacts with airframe dynamics through hub loads and motion, as well as with actuators providing blade pitch angle. Seat motion is the input to the pilot model which, in turn, yields the corresponding stick displacement to the actuator model. Other interactions like, for instance, the aerodynamic interference of main rotor with tail rotor and fuselage (main rotor wake impingement on the tail can cause airframe vibrations which, in turn, can couple with pilot control movement), are not taken into account because these are considered second-order effects in the RPC phenomena discussed in this paper.

In the following, the helicopter components models applied in the simulation tool developed for PAO analysis are described, with inclusion of the proposed finite-state formulation for rotor blades unsteady aerodynamics.

3.1 Main rotor aeroelastic modelling

Airloads transmitted from the main rotor to the airframe via the hub structure are determined by blade aeroelastic simulations based on a beam-like model. It derives from a nonlinear, bending-torsion formulation valid for slender, homogeneous, isotropic, nonuniform, twisted blades, undergoing moderate displacements[21-23]. The radial displacement is eliminated from the set of equations by solving it in terms of local tension, and thus the resulting structural operator consists of a set of coupled nonlinear differential equations governing elastic axis bending and blade torsion[24].

Coupling blade structural dynamics with aerodynamic loads modelling yields an aeroelastic integro-partial differential system of equations. These are spatially integrated through the Galerkin approach, with the description of elastic axis deformation and cross-section torsion as linear combinations of shape functions satisfying homogeneous boundary conditions. This yields a set of nonlinear, ordinary differential equations of the type[22,23].

$$\boldsymbol{M}(t)\ddot{\boldsymbol{q}}+\boldsymbol{C}(t)\dot{\boldsymbol{q}}+\boldsymbol{K}(t)\boldsymbol{q}=\boldsymbol{f}_{str}^{ex,nl}(\boldsymbol{q},\zeta,\xi,\boldsymbol{\theta}_c,t)+\boldsymbol{f}_{aer}(\boldsymbol{q},\zeta,\xi,\boldsymbol{\theta}_c,t) \quad \ldots (1)$$

https://doi.org/10.1017/S0001924000011155 Published online by Cambridge University Press

where $\mathbf{q}$ denotes the vector of Lagrangian coordinates (time-dependent coefficients of the shape function linear combinations), $\boldsymbol{\zeta}$ denotes airframe rigid-body linear and angular velocity components, $\boldsymbol{\xi}$ are airframe deformation dofs, whereas $\boldsymbol{\theta}_c$ collects the blade pitch controls. In addition, $\mathbf{M}$, $\mathbf{C}$, and $\mathbf{K}$ are time-periodic, mass, damping, and stiffness structural matrices representing the linear structural terms exclusively depending on blade Lagrangian coordinates (these become time independent for analysis of hovering flight conditions). Non-linear structural contributions and inertial terms due to external dofs (i.e., non-blade dofs) are collected in the forcing vector $\mathbf{f}_{str}^{ex,nl}$, whereas vector $\mathbf{f}_{aer}$ collects main rotor generalised aerodynamic forces (projection of aerodynamic loads onto shape functions).

Periodic aeroelastic responses in steady flight are determined through the harmonic balance approach[22,23]. It is a methodology suitable for the analysis of the asymptotic solution (as time goes to infinity) of differential equations forced by periodic terms. For stability analysis purposes, structural and inertial contributions in Equation (1) are linearised about a reference condition by a numerical small perturbation approach[23]. A similar linearisation process may be applied to aerodynamic loads, if described through a quasi-steady model; on the other hand, if an unsteady aerodynamic formulation is used for predicting airloads, then the identification of the corresponding contribution to the linearised aeroelastic operator requires the application of a reduced-order, state-space modelling approach.

3.2 State-space aerodynamic model for rotors in hovering and axial-flight

The linear, state-space model of rotor blade unsteady aerodynamic loads is obtained by the methodology introduced and validated in Ref. 14, and further applied in Ref. 15 to predict proprotor whirl-flutter stability boundaries. It is valid for rotorcraft flight conditions where the rotor wake remains symmetrically distributed about the shaft axis (namely, hovering and axial flight)[14]. As already stated, in the present analysis aerodynamic interactions between rotor wake and helicopter fuselage, and between main and tail rotors are neglected. Hub motion perturbations are assumed to be caused by rigid and elastic dynamics of the airframe.

The first step for identification of the state-space aerodynamic model consists in expressing the perturbation velocity of blade points in terms of blade and hub motion. Specifically, considering an observation frame of reference fixed with the unperturbed flow, the velocity of a blade point is expressed as the sum of velocities due to (*i*) rigid-body motion of the frame of reference rigidly connected to the hub, $\vec{v}_{rig}$, (*ii*) blade elastic deformations, $\vec{v}_{def}$, and (*iii*) pitch controls, $\vec{v}_{\theta}$, as given by

$$\begin{aligned}\vec{v}(\vec{x},t) &= \vec{v}_{rig}(\vec{x},t)+\vec{v}_{def}(\vec{x},t)+\vec{v}_{\theta}(\vec{x},t)\\ &= \vec{v}_{H}(t)+\vec{\omega}(t)\times(\vec{x}-\vec{x}_{H})+\vec{v}_{def}(\vec{x},t)+\vec{v}_{\theta}(\vec{x},t)\end{aligned} \quad \ldots (2)$$

where $\vec{v}_H$ denotes the hub velocity, $\vec{x}-\vec{x}_H$ is the distance vector between the hub and an arbitrary blade point, $\vec{x}$, whereas $\vec{\omega}$ is the rotor angular velocity. Then, in a frame of reference *Hxyz* rigidly connected to the undeformed rotor blades and centred at the rotor hub, the rigid-body motion velocity is represented as $\vec{v}_{rig}^{R}$ through the following linear combination of six time-independent vector shape functions, $\vec{\Psi}_n$;

$$\vec{v}_{rig}^{R}(\vec{x},t)=\sum_{n=1}^{6}v_n(t)\vec{\Psi}_n(\vec{x}) \quad \ldots (3)$$

where coefficients, v_n, correspond to the components of $\vec{v}_H$ and $\vec{\omega}$ in the *Hxyz* frame of reference (rotor generalised velocities)[14]. In addition, for each blade, velocity induced by elastic deformation

https://doi.org/10.1017/S0001924000011155 Published online by Cambridge University Press

is represented in *Hxyz* by;

$$\vec{v}_{def}^{R}(\vec{x},t) = \sum_{l=1}^{N_m} \dot{q}_l(t)\vec{\Phi}_l(\vec{x}) \qquad \ldots (4)$$

where scalars q_l are N_m generalised coordinates of the blade elastic motion, whilst vectors $\vec{\Phi}_l$ are derived by the shape functions chosen for blade deformation description in the Galerkin approach (they have time-independent components in the *Hxyz* rotor hub frame). Similarly to Equation (4), $\vec{v}_\theta$ is represented in *Hxyz* by linearly combining the blade pitch control with the vector representing the *Hxyz*-frame velocity distribution due to rotation about the feathering axis.

With rotor kinematics expressed in terms of time-independent space distribution functions, under the assumption of linear analysis, the perturbation generalised aerodynamic forces, $\mathbf{f}_b$, acting on each rotor blade in hovering or axial flight can be given by the following matrix expression in the frequency domain[14].

$$\tilde{\boldsymbol{f}}_b = \boldsymbol{E}_b(s)\tilde{\boldsymbol{w}} \qquad \ldots (5)$$

where **w** collects the variables through which the perturbed motion of rotor blades is described. If the blade aerodynamic matrix, $\mathbf{E}_b$, is determined by an aerodynamic solver capable of taking into account mutual aerodynamic interference among blades, airloads acting on each blade are influenced by deformation of all rotor blades. Thus, for a N_b-bladed rotor, **w** is a $(6 + N_b * N_m + 3)$ -element column matrix such that $\mathbf{w}^T = [\boldsymbol{v}^T\boldsymbol{q}^T\boldsymbol{\theta}_c^T]$, where **v**, **q** and $\boldsymbol{\theta}_c$ collect, respectively, 6 rotor generalised velocities, v_n, $N_b * N_m$ generalised coordinates of blades deformation, q_l, and N_b blade pitch control variables. If aerodynamic interference effects are not captured, the number of generalised coordinates in **w** is reduced to N_m; variables **v** disappear in hub-fixed conditions.

The aerodynamic forces collected in $\mathbf{f}_b$ include rotating-frame components of each blade contribution to hub loads, $\mathbf{f}_{hub}$ (i.e., those forcing airframe dynamics – see Section 3.3), as well as the generalised forces appearing in the blade aeroelastic formulation of Equation (1)).

Combining the contributions from all rotor blades and introducing the N_f-element column matrix, **f**, that collects the rotating-frame components of hub loads, $\mathbf{f}_{hub}$, along with generalised aerodynamic forces of all blades, $\mathbf{f}_{aer}$, yields the following frequency-domain, small-perturbation rotor aerodynamic loads model

$$\tilde{\boldsymbol{f}} = \begin{Bmatrix} \tilde{\boldsymbol{f}}_{hub} \\ \tilde{\boldsymbol{f}}_{aer} \end{Bmatrix} = \boldsymbol{E}(s)\tilde{\boldsymbol{w}} \qquad \ldots (6)$$

where **E** represents the rotor aerodynamic transfer-function matrix.

This model may be identified by any suitable frequency-domain aerodynamic solver. In the past, it has been successfully applied using strip-theory formulations based on sectional unsteady aerodynamic models with wake-inflow downwash corrections, as well as three-dimensional Boundary Element Method (BEM) solvers for unsteady potential flows[14,15]. In both cases, the entries of matrix **E** are transcendental functions of the complex frequency because of flow-memory effects due to wake vorticity released by each rotor blade trailing-edge (in sectional aerodynamic models these are represented by lift deficiency functions, as in Theodorsen's and Loewy's theories[25,26]. An aerodynamic operator of this type would give rise to an infinite-dimension state-space problem in time domain and would be not conveniently included in a dynamic model, particularly if applied to stability analysis and/or control purposes.

https://doi.org/10.1017/S0001924000011155 Published online by Cambridge University Press

Thus, the Reduced-Order Model (ROM) of the aerodynamic operator is identified by approximating **E** through a rational-matrix form. Techniques of this type are frequently used for aeroelastic analysis of fixed wings[16,27] and have already been applied to the stability analysis of isolated rotors[15,28]. The specific approach used here stems from the methodology presented in Ref. 29 that introduces the following rational-matrix approximation;

$$\boldsymbol{E}(s) \approx s^2 \boldsymbol{A}_2 + s\boldsymbol{A}_1 + \boldsymbol{A}_0 + \boldsymbol{C}\left[s\boldsymbol{I} - \boldsymbol{A}\right]^{-1}\boldsymbol{B} \qquad \ldots (7)$$

where matrices $\mathbf{A}_2$, $\mathbf{A}_1$ and $\mathbf{A}_0$ have dimensions $[N_r \times (6 + N_b * N_m + 3)]$. In addition, **A** is a square matrix with dimensions $[N_a \times N_a]$, **C** is a $[N_f \times N_a]$ matrix, and **B** has dimensions $[N_a \times (6 + N_b * N_m + 3]$, with N_a denoting the number of poles introduced.

Then, combining Equation (6) with Equation (7) and transforming into the time domain yields the following constant-coefficient expression of the aerodynamic hub loads and blade generalised forces;

$$\begin{aligned} \boldsymbol{f}(t) &= \boldsymbol{A}_2\ddot{\boldsymbol{w}} + \boldsymbol{A}_1\dot{\boldsymbol{w}} + \boldsymbol{A}_0\boldsymbol{w} + \boldsymbol{C}\boldsymbol{r} \\ \dot{\boldsymbol{r}} &= \boldsymbol{A}\boldsymbol{r} + \boldsymbol{B}\boldsymbol{w} \end{aligned} \qquad \ldots (8)$$

where **r** is the column matrix that collects the N_a additional aerodynamic states associated to the poles introduced in the approximated aerodynamic matrix (consequence of flow-memory effects affecting matrix **E**).

The final step of the rotor aerodynamic state-space ROM identification process consists in expressing the rotor rigid-body velocities, **v**, in terms of helicopter motion as follows,

$$\boldsymbol{v}(t) = \boldsymbol{K}_1(t)\zeta + \boldsymbol{K}_2(t)\dot{\xi} \qquad \ldots (9)$$

where $\mathbf{K}_1$ and $\mathbf{K}_2$ are periodic matrices depending on helicopter geometry and airframe modal shapes. These two matrices are time dependent because of the relative motion between the hub rotating frame of reference, *Hxyz* (where rotor velocity components are defined), and the non-rotating frame of reference where airframe rigid-body motion and deformation are represented through variables ζ and ξ. Combining Equation (9) with Equation (8) yields

$$\begin{aligned} \boldsymbol{f}_T(t) &= \boldsymbol{D}_2(t)\ddot{\boldsymbol{y}} + \boldsymbol{D}_1(t)\dot{\boldsymbol{y}} + \boldsymbol{D}_0(t)\boldsymbol{y} + \boldsymbol{C}\boldsymbol{r} \\ \dot{\boldsymbol{r}} &= \boldsymbol{A}\boldsymbol{r} + \boldsymbol{H}_1(t)\dot{\boldsymbol{y}} + \boldsymbol{H}_0(t)\boldsymbol{y} \end{aligned} \qquad \ldots (10)$$

where; $\mathbf{y}^T = \left[\zeta^T \xi^T \mathbf{q}^T \theta_c^T\right]$

The proposed model allows for time-domain evaluation of rotor blade aerodynamic loads as explicit functions of helicopter dynamics state variables, as well as of a finite number of additional (aerodynamic) states. Although coefficients appearing in this state-space ROM are periodic functions, its identification process relies on outcomes of a frequency-domain aerodynamic solver, thanks to the assumption of axially developed wake shape[14]. Coupled with rotor and airframe dynamics equations, it provides a comprehensive helicopter state-space model suitable for eigenvalue stability analysis (through the Floquet theory) and control law design. Note that, the level of accuracy of airloads predicted by the presented state-space ROM is strictly related to the level of accuracy of the aerodynamic frequency-domain solver applied in the identification process.

https://doi.org/10.1017/S0001924000011155 Published online by Cambridge University Press

3.3 Airframe modelling

Past work has demonstrated that airframe rigid-body and deformation dynamics play a crucial role in RPC onset[7]. In particular, in PAO analysis the main contribution to the pilot seat vibration comes from airframe deformations.

Airframe rigid-body dynamics is described through a standard six-degree of freedom model forced by main rotor and tail rotor loads, with Euler angles taking into account spatial orientation. Its linearisation about an arbitrary trimmed steady flight condition yields (see, for instance Ref. 30);

$$\begin{aligned}
&\dot{u} - r_0 v + q_0 w + w_0 q - v_0 r + g\mathrm{Cos}(\theta_0)\theta - X/M_f &&= 0\\
&\dot{v} + r_0 u - p_0 w - w_0 p + u_0 r - g\mathrm{Cos}(\phi_0)\mathrm{Cos}(\theta_0)\phi + g\mathrm{Sin}(\phi_0)\mathrm{Sin}(\theta_0)\theta - Y/M_f &&= 0\\
&\dot{w} - q_0 u + p_0 v + v_0 p - u_0 q + g\mathrm{Sin}(\phi_0)\mathrm{Cos}(\theta_0)\phi + g\mathrm{Cos}(\phi_0)\mathrm{Sin}(\theta_0)\theta - Z/M_f &&= 0\\
&\dot{p} - I^x_{xz}\dot{r} + (I^x_{zz} - I^x_{yy})r_0 q + (I^x_{zz} - I^x_{yy})q_o r - I^x_{xz} p_0 q - I^x_{xz} q_0 pq - L/I_{xx} &&= 0\\
&\dot{q} + (I^y_{xx} - I^y_{zz})r_0 p + (I^y_{xx} - I^y_{zz})p_0 r + 2I^y_{xz}(p_0 p - r_0 r) - M/I_{yy} &&= 0\\
&\dot{r} - I^z_{zx}\dot{p} + (I^z_{yy} - I^z_{xx})p_0 q + (I^z_{yy} - I^z_{xx})q_0 p + I^z_{xz} r_0 q + I^z_{xz} q_0 r - N/I_{zz} &&= 0\\
&\dot{\phi} - \psi\mathrm{Sin}(\theta_0) - p &&= 0\\
&\dot{\theta}\mathrm{Cos}(\phi_0) + \psi\mathrm{Sin}(\phi_0)\mathrm{Cos}(\theta_0) - q &&= 0\\
&\dot{\theta}\mathrm{Sin}(\phi_0) - \psi\mathrm{Cos}(\phi_0)\mathrm{Cos}(\theta_0) + r &&= 0
\end{aligned} \quad \ldots (11)$$

where M_f is the helicopter mass, $I^k_{i,j} = I_{ij}/I_{kk}$ denotes nondimensional components of airframe inertia matrix and g is the gravity acceleration. Airframe kinematics are described through variables u,v,w and p,q,r that are, respectively, the components of centre-of-mass velocity and airframe angular velocity in a body-fixed frame of reference (collected in the column matrix $\boldsymbol{\zeta}$), with the inclusion of ϕ,θ,ψ denoting roll, pitch and yaw orientation angles, respectively. Furthermore, X,Y,Z and L,M,N are, respectively, the components of force and centre-of-gravity moment resulting from the combination of loads transmitted by main rotor and tail rotor, along with fuselage aerodynamic loads (with the last two contributions predicted through steady aerodynamics models). Subscript 0 identifies values of trimmed state variables.

Airframe deformation is described through a linear combination of mode shapes with coefficients, $\boldsymbol{\xi}$ (Lagrangian coordinates), governed by the following ordinary differential equations;

$$\boldsymbol{M}_\xi \ddot{\boldsymbol{\xi}} + \boldsymbol{C}_\xi \dot{\boldsymbol{\xi}} + \boldsymbol{K}_\xi \boldsymbol{\xi} = \boldsymbol{f}_\xi \quad \ldots (12)$$

where $\mathbf{M}_\xi$, $\mathbf{C}_\xi$ and $\mathbf{K}_\xi$ are mass, damping and stiffness matrices determined by finite-element-method analysis of the unconstrained airframe[7]. Forcing terms $\mathbf{f}_\xi$ are the generalised forces obtained by projection of main rotor and tail rotor loads onto mode shapes.

3.4 Actuator dynamics modelling

As mentioned in Section 1, the present work focuses attention on PAO phenomena driven by inadvertent movement of the collective resulting from unintentional pilot body motion due to vertical accelerations (vertical bouncing). To this purpose, swashplate actuators dynamics concerning pilot's collective pitch control are modelled by the following second-order transfer function between collective stick rotation, α, and blades collective pitch, θ_0,

https://doi.org/10.1017/S0001924000011155 Published online by Cambridge University Press

$$\ddot{\theta}_0 + 2D\omega_\theta\dot{\theta}_0 + \omega_\theta^2\theta_0 - \omega_\theta^2\alpha = 0 \quad \ldots (13)$$

where ω_θ and D are, respectively, model equivalent frequency and relative damping (see also Ref. 7). Cyclic pitch and pedal controls have not been included in the model because they have been shown to have a weak influence on vertical bounce phenomena[7].

3.5 Pilot modelling

In RPC analyses, the pilot feedthrough is the link between rotorcraft motion and control stick movement. RPC phenomena in which aeroelastic effects play an important role (PAO events) are characterised by the dynamic response in the 2–8Hz range (see Fig. 1), where the pilot feedthrough is dominated by involuntary (passive) body responses, with negligible contribution from voluntary actions.

Several passive pilot models have been proposed in the last decades, moving from that introduced by Mayo[20] to those more recently presented in Refs 31-33. In most of these works, the pilot models are derived as SISO transfer functions identified from experiments by shaking pilots operating for different tasks in several workload conditions. In Ref. 33, a MIMO pilot behaviour is numerically simulated through a multibody solver. Since the main RPC application of the helicopter modelling presented in this paper concerns vertical bouncing analysis, pilot feedthrough is described by Mayo's passive pilot model.

It is expressed in terms of the following transfer functions between seat acceleration and collective control (stick) acceleration, for pilots of different weight (ectomorphic-lighter and mesomorphic-heavier, respectively);

$$H_{ecto} = \frac{\tilde{a}_0}{\tilde{a}_z} = G\frac{5\cdot19s + 452\cdot3}{s^2 + 13\cdot7s + 452\cdot3} \quad \ldots (14)$$

$$H_{meso} = G\frac{4\cdot02s + 555\cdot4}{s^2 + 13\cdot31s + 555\cdot4} \quad \ldots (15)$$

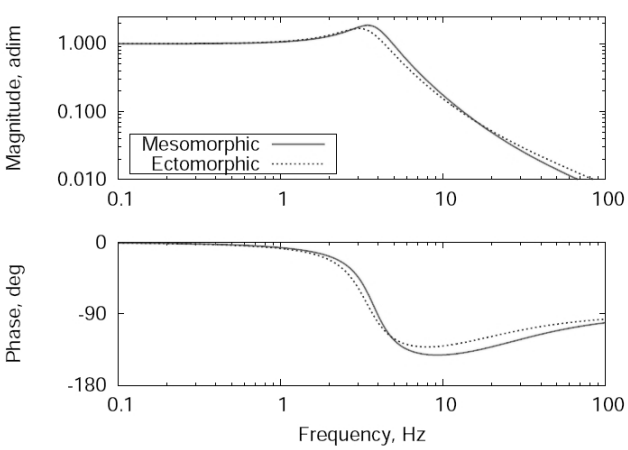


Figure 3. Mayo transfer functions between seat and control accelerations.

https://doi.org/10.1017/S0001924000011155 Published online by Cambridge University Press

where a_o and a_z denote absolute vertical acceleration of pilot hand and pilot seat, respectively, whereas G is the amplification factor (gain).

These two transfer functions (depicted in Fig. 3 for $G = 1$) present two poles and one zero that are assumed to be independent of the reference angle of the collective control stick. The dependence of the transfer functions on the pilot operating condition is introduced by Mayo through the relation between gain and reference stick position illustrated in Fig. 4, which has been derived from the 3Hz response amplification observed experimentally for different reference stick positions[20]. However, the accuracy of the description of pilot feedthrough dependence on reference collective control angular positions as provided by Equations (14) and (15) combined with the information in Fig. 4 is poor. Indeed, the change in the attitude of the involved limbs would modify the transfer functions not only in terms of amplification factor, but also in terms of poles and zeros[7].

Finally, in order to connect Equations (14) and (15) with Equation (13), these have to be transformed to provide the collective stick (relative) rotation as a function of the seat vertical acceleration. This is obtained by the following expression;

$$\tilde{\alpha} = \frac{1}{r_{st}} \frac{1}{s^2} (\tilde{a}_0 - \tilde{a}_z) = \frac{1}{r_{st}} \frac{1}{s^2} (H - 1) \tilde{a}_z \qquad \ldots (16)$$

where r_{st} is the collective stick length. Note that, Equation (16) describes a non-physical behaviour for frequencies below 1Hz (i.e., in the intentional pilot behaviour range). This is due to the fact that Mayo's experiments concerned measurements ranging from 1 to 6Hz, without inclusion of pilot's intentional actions to compensate unintentional low-frequency stick motion perceived by the pilot. Indeed, the presence of two integration poles yields a divergent behaviour of the transfer functions as s tends to zero (in order to overcome this problem, a modification of the integration poles is suggested in Ref. 10).

Seat acceleration, a_z, is determined through a combination of rigid-body motion and deformation of the airframe.

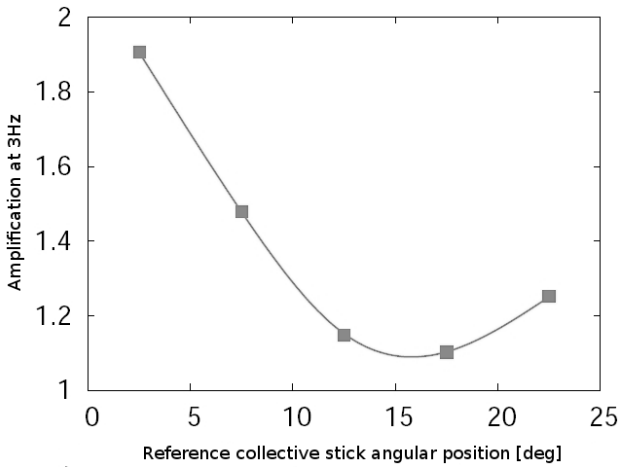


Figure 4. Transfer function gain *vs* reference stick position.

https://doi.org/10.1017/S0001924000011155 Published online by Cambridge University Press

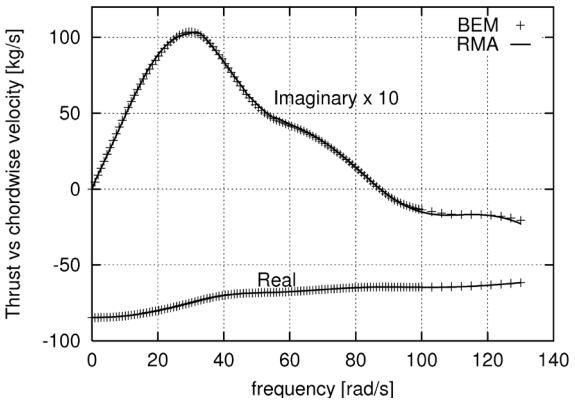


Figure 5. RMA of transfer function between v_1 and thrust of blade 1.

4.0 NUMERICAL RESULTS

In this section, results concerning the validation of the aerodynamic state-space ROM outlined above are first presented, followed by the application to RPC/PAO problems.

The assessment of the accuracy of the present state-space aerodynamic ROM has been performed in the past, as shown in Ref. 14. Here, some of the results presented in Ref. 14 are included for the sake of completeness. They regard a three-bladed proprotor in cruise flight. Figure 5 shows values of the transfer function relating the hub velocity component, v_1 (namely, the component in the rotor disk plane that is orthogonal to blade 1 axis), and the thrust acting on blade 1. Specifically, it presents the comparison between the values computed by the frequency-domain BEM potential-flow solver of Ref. 34, and those provided by the corresponding rational-matrix approximation (RMA).

In the frequency range examined, the agreement between the two solutions proves that the accuracy of the RMA is excellent. Note that, the wavy behaviour in Fig. 5 is caused by the vorticity in the rotor wake. Indeed, the inflow on the rotor disk due to the vorticity convected past the trailing edges generates memory effects on airloads that are described by the inclusion of suitable poles in the corresponding transfer functions (as already mentioned, in the unsteady aerodynamics of aerofoils, these phenomena are described by transcendental lift deficiency functions, as in Theodorsen's[25] and Loewy's[26] theories). The wavy behaviour of the aerodynamic transfer functions sharpens when the wake remains closer to the blades (see, for instance, Ref. 28 where the RMA validation is presented for a hovering rotor). It has been observed that, for all the transfer functions in matrix **E**, the level of accuracy of the RMA is comparable to that of results in Fig. 5.

Then, the accuracy of the state-space ROM derived from the RMA of the transfer-function matrix is assessed. To this purpose, considering the same flight condition examined for the results in Fig. 5, the proprotor is assumed to be rigidly connected (through a rigid pylon, as in a tiltrotor configuration) to the tip of a wing undergoing flap and torsion deformation; rotor blades are assumed to be deformable, as well. Wing and blades deformations are imposed to be damped, multi-harmonic oscillatory functions of time, tending to a harmonic behaviour asymptotically (see Ref. 14 for details). The aerodynamic forces associated with this motion are evaluated both by applying the state-space aerodynamics presented in this work and through the time-domain BEM potential-flow solver[34]. Figure 6 shows the thrust force acting on blade 1 computed by both approaches: these results are in excellent agreement, thus demonstrating the very good accuracy of the aerodynamic loads predicted by the state-space model.

https://doi.org/10.1017/S0001924000011155 Published online by Cambridge University Press

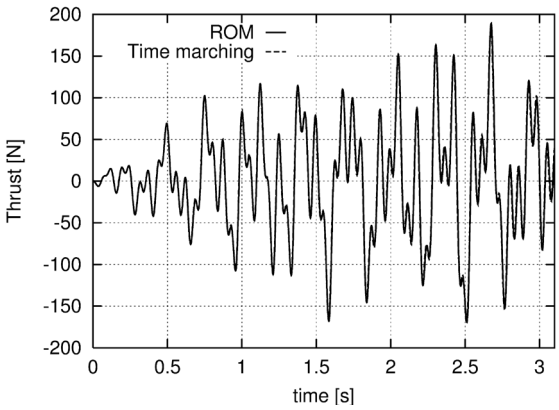


Figure 6. Blade thrust perturbation due to hub/blade motion.

Next, RPC/PAO phenomena are investigated by application of the state-space ROM aerodynamics based on the frequency-domain BEM potential-flow solver[34]. The test case chosen is the Bo–105 helicopter in hover flight at sea level, with a mass of 2,200kg, that corresponds to trim collective angle $\theta_0 = 9°$ (for further details about the Bo–105 model, see Refs 5, 7).

The numerical test is performed through analysis of eigenvalues, for the gain, G, of the ectomorphic pilot transfer function increasing from 0 (out-of-the-loop pilot) to 1·4; note that $G > 1$ values are investigated to take into account different arm/stick configurations, as shown in Ref. 20. Since helicopter dynamics are governed by periodic equations, the eigenanalysis is performed by the Floquet theory. This provides multi-frequency eigenvalues and hence, in the following, the frequency associated to any eigenvalue is the dominant one.

Assuming a rigid-blade rotor and using sectional, quasi-steady aerodynamics with static inflow downwash correction, Fig. 7 shows the damping of the three helicopter dynamics eigenvalues most affected by the pilot transfer function gain. No unstable poles arise as the pilot gain increases. Nevertheless, in the mid-frequency range (3-4Hz), the 'pilot mode' tends to become less stable, while the first airframe elastic mode becomes more stable, like the zero-frequency heave subsidence, which is the rigid-body mode mostly affected by the pilot feedthrough. The same analysis performed by the state-space aerodynamic ROM provides the results presented in Fig. 8. The overall behaviour is quite similar to that shown in Fig. 7 revealing that, as expected, in the absence of blade deformations, quasi-steady aerodynamics is fully capable of capturing the dominant features of RPC phenomena. It is worth noting that spiral mode damping is scarcely affected by pilot gain, and it is not presented in Fig. 7.

Next, blade deformations are included in the helicopter modelling. In comparison with the rigid rotor analysis, the application of the state-space unsteady aerodynamic model yields different PAO predictions with respect to those provided by quasi-steady aerodynamics. Specifically, the comparison between Figs 9 and 10 (where only the most critical mode dampings are shown) reveals that, because of pilot feedthrough inclusion, unsteady aerodynamics predicts a more severe destabilisation of the system that concerns, in particular, the pilot/airframe mode and, partially, the low-frequency (about 0·5Hz) phugoid mode. Instead, quasi-steady aerodynamics yields a weak 'dutch roll' instability, as well as a moderate instability of the first airframe elastic mode which strongly couples with pilot dynamics. This difference in the predicted dynamic behaviours is due to the aerodynamic poles and three-dimensional/interactional effects of the

https://doi.org/10.1017/S0001924000011155 Published online by Cambridge University Press

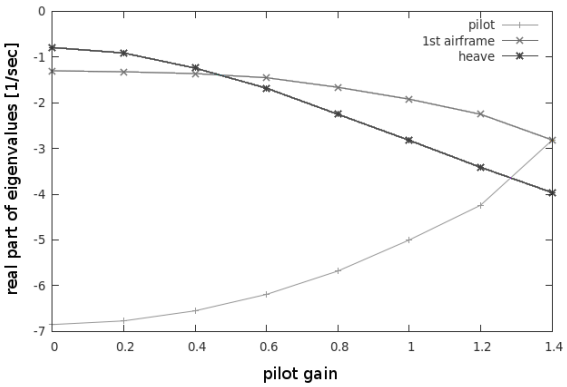


Figure 7. Pilot-in-the-loop effect on helicopter-pilot damping: rigid-blade rotor, sectional quasi-steady aerodynamics.

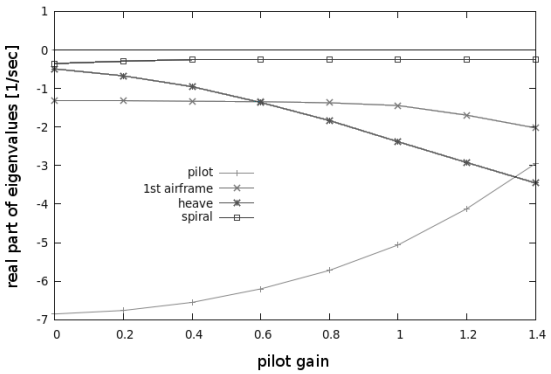


Figure 8. Pilot-in-the-loop effect on helicopter-pilot damping: rigid-blade rotor, state-space ROM aerodynamics.

state-space ROM, which affect main rotor aeroelastic responses. Aerodynamic poles may couple significantly with some of the helicopter modes, but, due to the nature of the ROM identification process, a detailed physical description of these couplings is an impossible task. It is worth noting that the unstable behaviour induced by the inclusion of the pilot in the loop is strongly dependent on the pilot model. While in this paper the focus is on the assessment of aerodynamic modelling on RPC analysis, the identification of a reliable/realistic pilot model is an open question still under investigation by researchers[2,31,32,35]. In particular, pilot task, workload and skill, along with cockpit design may significantly affect pilot response, and hence have an effect on PAO insurgency. Numerical investigations aimed at assessing the role of some of these factors in RPC analyses are discussed in Refs 31, 36, 37.

Finally, Figs 11 and 12 show helicopter gust responses with and without pilot in the loop, predicted by the application of state-space rotor unsteady aerodynamics. The interest in gust response is twofold: firstly, the assessment of the impact of the pilot on load factor response, that may be of help in designing gust alleviation systems; secondly, the estimation of the potential onset of strong gust responses that might trigger nonlinear (category III) RPC instabilities. Here, Fig. 11 illustrates the transfer functions between lateral gust velocity and vertical seat

https://doi.org/10.1017/S0001924000011155 Published online by Cambridge University Press

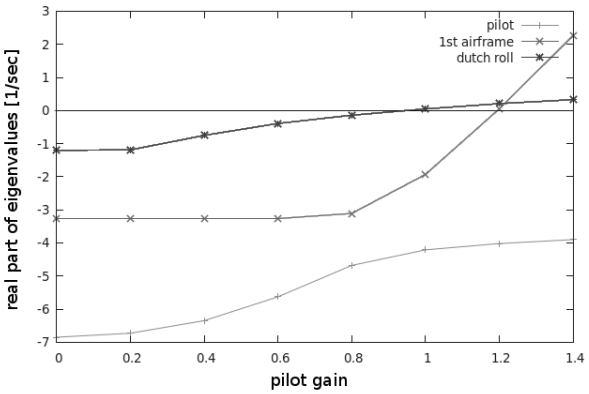


Figure 9. Pilot-in-the-loop effect on helicopter-pilot damping: deformable-blade rotor, sectional quasi-steady aerodynamics.

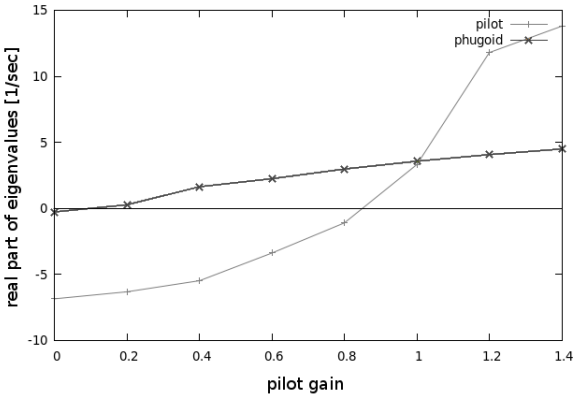


Figure 10. Pilot-in-the-loop effect on helicopter-pilot damping: deformable-blade rotor, state-space ROM aerodynamics.

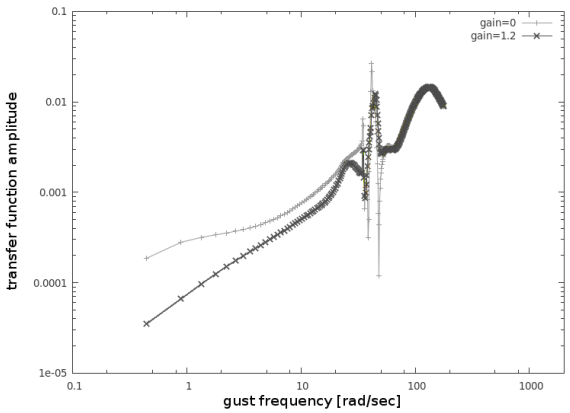


Figure 11. Transfer function between lateral gust velocity and vertical seat acceleration.

https://doi.org/10.1017/S0001924000011155 Published online by Cambridge University Press

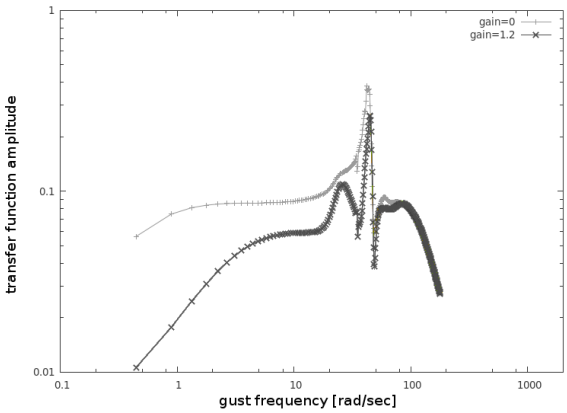


Figure 12. Transfer function between vertical gust velocity and vertical seat acceleration.

acceleration, whilst Fig. 12 depicts the transfer functions between vertical gust velocity and vertical seat acceleration (continuous, purely periodic gusts are considered). As expected, the response to lateral gust is significantly smaller than that to vertical gust, with one order of magnitude of difference between peaks (the biggest difference appearing at the lowest frequencies is not reliable in that, as stated in Section 3.5, Mayo's transfer function provides non-physical outcomes in that range of frequencies). Moreover, these figures confirm the results presented in Ref. 38 concerning a tiltrotor analysis: pilot and helicopter transfer functions phases are such that pilot-in-the-loop effects are beneficial in terms of load factor induced by gusts.

5.0 CONCLUSIONS

The effect of rotor aerodynamic models of different accuracy and complexity on the prediction of aeroelastic RPC phenomena has been examined. In the past, only widely-used quasi-steady sectional aerodynamic models with wake-inflow downwash corrections were applied in this kind of applications, with more attention focused on structural and BDFT modelling. A linear, time-periodic, state-space aerodynamic model taking into account three-dimensional, unsteady effects, as well as interaction effects among blades, has been identified through frequency responses provided by a BEM potential-flow solver. This model, suitable for rotors in axial-flow, has been coupled with rotor and airframe structural dynamics models. The inclusion in the loop of a passive pilot model has provided a comprehensive state-space tool that has been applied to stability and response analyses of a piloted hovering helicopter. These analyses have shown that, especially in the presence of blade and airframe deformations, three-dimensional, unsteady-flow effects play a significant role in RPC/PAO phenomena predictions: indeed, the state-space aerodynamic model predicts PAO instability at a value of pilot gain that is about 30% lower than that determined through the solver based on quasi-steady sectional aerodynamic modelling. In addition, it has been shown that unsteady aerodynamic effects play a rather significant role even in vehicle rigid-body mode dynamics, mainly due to the coupling with rotor blade aeroelasticity. Similar RPC predictions have been provided by quasi-steady and unsteady aerodynamics, when main rotor is assumed to be rigid. Finally, the influence of the pilot-in-the-loop on gust responses has been investigated. Both for vertical and lateral gusts, the passive pilot produces a beneficial effect on the load

https://doi.org/10.1017/S0001924000011155 Published online by Cambridge University Press

factor evaluated at the pilot seat, in that it induces reduction of peak and mean response. Future developments might include: (*i*) extension and application of the state-space unsteady aerodynamic model to RPC phenomena in forward flight conditions; (*ii*) extension of the comprehensive helicopter model to applications concerning the analysis of instabilities involving large fuselage motion and strong aerodynamic interactions between rotors and fuselage (for which simpler semi-analytical aerodynamic models are certainly unsuitable); (*iii*) validation of the outcomes derived from numerical predictions with the outcomes of a pilot-in-the-loop flight simulator test campaign.

ACKNOWLEDGEMENTS

The research leading to these results has been partially funded by the European Community's Seventh Framework Programme (FP7/2007-2013) under grant agreement N. 266073.

REFERENCES

1. STRELOW, H. Pilot activated oscillations rotorcraft pilot coupling. Technical Report Helicopter Exploratory Group EG-22, GARTEUR EG report, April 2004.
2. PAVEL, D.M., JUMP, M., DANG-VU, B., MASARATI, P., GENNARETTI, M., IONITA, A., ZAICHIK, L. and SMAILI, H., QUARANTA, G., YILMAZ, D., JONES, M., SERAFINI, J. and MALECKI, J. Adverse rotorcraft pilot couplings-past, present and future challenges, *Progress in Aerospace Sciences*, 2013, **62**, pp 1-51.
3. PAVEL, M.D., YILMAZ, D., DANG VU, B., JUMP, M., JONES, M. and LU, L. Adverse rotorcraft-pilot couplings – modelling and prediction of rigid body rpc – sketches from the work of European project Aristotel. In Proceedings of 39th European Rotorcraft Forum, Moscow, Russia, September 2013.
4. GENNARETTI, M., MOLICA COLELLA, M., SERAFINI, J., DANG-VU, B., MASARATI, P., QUARANTA, G., MUSCARELLO, V., JUMP, M., JONES, M., LU, L., IONITA, A., FUIOREA, I., MIHAILA-ANDRES, M. and STEFAN, R. Anatomy, modelling and prediction of aeroservoelastic rotorcraft pilot-coupling. In Proceedings of 39th European Rotorcraft Forum, Moscow, Russia, September 2013.
5 DIETERICH, O., GÖTZ, J., DANG-VU, B., HAVERDINGS, H., MASARATI, P., PAVEL, M., JUMP, M. and GENNARETTI, M. Adverse rotorcraft-pilot coupling: Recent research activities in Europe. In Proceedings of the 34th European Rotorcraft Forum, Liverpool, UK, September 2008.
6. GENNARETTI, M., MASARATI, P., QUARANTA, G. and SERAFINI, J. Numerical investigation of aeroservoelastic rotorcraft-pilot coupling. In Proceedings of XIX Congresso Nazionale AIDAA, Forlí, Italy, September 2007.
7 SERAFINI, J., GENNARETTI, M., MASARATI, P., QUARANTA, G. and DIETERICH, O. Aeroelastic and biodynamic modeling for stability analysis of rotorcraft-pilot coupling phenomena. In Proceedings of 34th European Rotorcraft Forum, Liverpool, UK, September 2008.
8. MASARATI, P., QUARANTA, G., GENNARETTI, M. and SERAFINI, J. Aeroelastic investigation of rotorcraft-pilot coupling)rpc) by coupled BEM/multibody analysis. In Proceedings of 37th European Rotorcraft Forum, Gallarate, Italy, September 2011.
9. SERAFINI, J., MOLICA COLELLA, M. and GENNARETTI, M. A finite-state aeroelastic model for rotorcraft pilot-assisted-oscillations analysis. In Proceedings of 38th European Rotorcraft Forum, Amsterdam, The Netherlands, September 2012.
10. GENNARETTI, M., SERAFINI, J. MASARATI, P. and QUARANTA, G. Effects of biodynamic feedthrough in rotorcraft/pilot coupling: collective bounce case, *J Guidance Control and Dynamics*, 2013, **36**, (6), pp 1709-1721.
11. MASARATI, M., QUARANTA, G. and JUMP, M. Experimental and numerical helicopter pilot characterization for aeroelastic rotorcraft-pilot couplings analysis. *Proceedings of the Institution of Mechanical Engineers, Part G: J Aerospace Engineering*, 2013, **227**, (1), pp 124-140.
12. MASARATI, M., G. QUARANTA, G., LU, L. and JUMP, M. A closed loop collective bounce adverse aeroelastic rotorcraft-pilot coupling experiment, *J Sound and Vibration*, 2014, **333**, (1), pp 307-325.
13. SERAFINI, J., MOLICA COLELLA, M. and GENNARETTI, M. A finite-state aeroelastic model for rotorcraft-pilot coupling analysis, *CEAS Aeronaut J*, 2014, **5**, (1), pp 1-11.

https://doi.org/10.1017/S0001924000011155 Published online by Cambridge University Press

14. GENNARETTI, M. and GRECO, L. A time-dependent coefficient reduced-order model for unsteady aerodynamics of proprotors, *J Aircr*, 2005, **42**, (1), pp 138-147.
15. GENNARETTI, M. and GRECO, L. Whirl flutter analysis of prop-rotors using unsteady aerodynamics reduced-order models, *Aeronaut J*, 2008, **112**, (1131), p 233-242.
16. KARPEL, M. Design for the active flutter suppression and gust alleviation using state-space aeroelastic modeling, *J Aircr*, 1982, **19**, (3), pp 221-227.
17. VEPA, R. On the use of Padé approximants to represent unsteady aerodynamic loads for arbitrarily small motions of wings. (AIAA Paper 76-17), January 1976.
18. ROGER, K.L. Airplane math modeling methods for active control design. Technical Report AGARD-CP-228, AGARD, August 1977.
19. EDWARDS, J.W., ASHLEY, H. and BREAKWELL, J.V. Unsteady aerodynamic modeling for arbitrary motions. *AIAA J*, 1979, **17**, (4), pp 365-374.
20. MAYO, J.R. The involuntary participation of a human pilot in a helicopter collective control loop. In Proceedings of 15th European Rotorcraft Forum, Amsterdam, The Netherlands, September 1989.
21. HODGES, D.H. and DOWELL, E.H. Nonlinear equation for the elastic bending and torsion of twisted nonuniform rotor blades. NASA Technical Note TN D-7818, NASA, 1974.
22. GENNARETTI, M. and BERNARDINI, G. Aeroelastic response of helicopter rotors using a 3D unsteady aerodynamic solver, *Aeronaut J*, 2006, **110**, (1114), pp 793-801.
23. BERNARDINI, G., SERAFINI, J., MOLICA COLELLA, M. and GENNARETTI, M. Analysis of a structural-aerodynamic fully-coupled formulation for aeroelastic response of rotorcraft, *Aerospace Science and Technology*, 2013, **29**, (1), pp 175-184.
24. HODGES, D.H. and ORMISTON, R.A. Stability of elastic bending and torsion of uniform cantilever rotor blades in hover with variable structural coupling. NASA Technical Note TN D-8192, NASA, 1976.
25. THEODORSEN, T. General theory of aerodynamic instability and the mechanism of flutter. NACA Report 496, NACA, 1935, 24
26. LOEWY, R.G. A two-dimensional approximation of unsteady aerodynamics of rotary wings, *J Aeronautical Sciences*, 1957, **24**, (2), pp 81-93.
27. GENNARETTI, M. and PONZI, C. Finite-state aerodynamic modelling for gust load alleviation of wing-tail configurations, *Aeronaut J*, 1999, **103**, (1021), pp 147-158.
28. GENNARETTI, M. CORBELLI, A. and MASTRODDI, F. A comparison among some aeroelastic models for the stability analysis of a flap-lag-torsion helicopter rotor in hover. In Proceedings of 26th European Rotorcraft Forum, The Hague, The Netherlands, September 2000.
29. MORINO, L., MASTRODDI, F., DE TROIA, R., GHIRINGHELLI, G.L. and MANTEGAZZA, P. Matrix fraction approach for finite-state aerodynamic modeling. *AIAA J*, 1995, 180, **33**, (4), pp 703, **711**.
30. PADFELD, G.D. *Helicopter Fight Dynamics*, Blackwell Science Ltd, Oxford, 2 ed, 2007.
31. VENROOIJ, J. MULDER, M. ABBINK, D.A. VAN PAASSEN, M.M.. MULDER, M. F.C.T. *van der Helm*, and H.H *Bultho*. Mathematical biodynamic feedthrough model applied to rotorcraft. *IEEE Transactions on Cybernetics*, 2013, **44**, (7), pp 1125-1138.
32. VENROOIJ, J., ABBINK, D.A., MULDER, M., VAN PAASSEN, M.M., MULDER, M., VAN DER HELM, F.C.T. and BULTHOFF, H.H. A biodynamic feedthrough model based on neuromuscular principles, *IEEE Transactions on Cybernetics*, 2013, **44**, (7), pp 1141-1154.
33. MASARATI, P., QUARANTA, G. and ZANONI, A. Dependence of helicopter pilots biodynamic feedthrough on upper limbs muscular activation patterns, *Proceedings of the Institution of Mechanical Engineers, Part K: J Multi-body Dynamics*, 2013, **227**, (4), pp 344.
34. MORINO, L. and GENNARETTI, M. Computational Nonlinear Mechanics in Aerospace Engineering, volume **146** of Aeronautics & Astronautics AIAA Series, chapter Boundary integral equation methods for aerodynamics, pp 279-320. S.N. Atluri, 1992.
35. ZAICHIK, L., YASHIN, Y., DESYATNIK, P., MASARATI, P., QUARANTA, G., PAVEL, M.D. VENROOIJ, J. and SMAILI, H. Biodynamic pilot modelling for aeroelastic a/rpc. In Proceedings of 39th European Rotorcraft Forum, Moscow, Russia, September 2013.
36. QUARANTA, G., MASARATI, P. and VENROOIJ, J. Impact of pilots' biodynamic feedthrough on rotorcraft by robust stability, *J Sound and Vibration*, 2013, **332**, (20), pp 4948-4962.
37. QUARANTA, G. TAMER, A. MUSCARELLO, V. MASARATI, P. GENNARETTI, M. SERAFINI, J. and MOLICA COLELLA, M. A finite-state aeroelastic model for rotorcraft-pilot coupling analysis, *CEAS Aeronaut J*, 2014, **5**, (1), pp 29-39.
38. MURO, D., MOLICA COLELLA, M., SERAFINI, J. and GENNARETTI, M. An optimal control approach for alleviation of tiltrotor gust response, *Aeronaut J*, 2012, **116**,(1180), pp 651-666.

https://doi.org/10.1017/S0001924000011155 Published online by Cambridge University Press